Thickness and Birefringence of Healthy Retinal Nerve Fiber Layer Tissue Measured with Polarization-Sensitive Optical Coherence Tomography

Barry Cense,[1] *Teresa C. Chen,*[2] *B. Hyle Park,*[1] *Mark C. Pierce,*[1] *and Johannes F. de Boer*[1]

Purpose. Thinning of the retinal nerve fiber layer and changes in retinal nerve fiber layer (RNFL) birefringence may both precede clinically detectable glaucomatous vision loss. Early detection of RNFL changes may enable treatment to prevent permanent loss of vision. Polarization-sensitive optical coherence tomography (PS-OCT) can provide objective information on RNFL thickness and birefringence.

Methods. PS-OCT scans around the optic nerve head (ONH) of two healthy young volunteers were made using 10 concentric circles of increasing radius. Both the mean RNFL thickness and mean retinal nerve fiber birefringence for each of 48 sectors on a circle were determined with data analysis.

Results. Both the RNFL thickness and birefringence varied as a function of sector around the ONH. The RNFL became thinner with increasing distance from the ONH. In contrast, the birefringence did not vary significantly as a function of radius.

Conclusions. Birefringence of healthy RNFL is constant as a function of scan radius but varies as a function of position around the ONH, with higher thickness values occurring superior and inferior to the ONH. Measured double-pass phase retardation per unit depth around the ONH ranged between 0.10 and 0.35 deg/μm, equivalent to birefringences of 1.2×10^{-4} and 4.1×10^{-4} respectively, measured at a wavelength of 840 nm. Consequently, when a spatially constant birefringence around the ONH is assumed, the conversion of scanning laser polarimetry (SLP) phase-retardation measurements to RNFL thickness may yield incorrect values. The data do not invalidate the clinical value of a phase-retardation measurement, but affect the conversion of phase retardation to RNFL thickness. (*Invest Ophthalmol Vis Sci.* 2004;45:2606–2612) DOI: 10.1167/iovs.03-1160

Glaucoma is the world's second leading cause of blindness. The disease causes damage to the retinal ganglion cells, resulting in thinning of the retinal nerve fiber layer (RNFL). In addition, nerve fiber layer tissue loss may be preceded by changes in birefringence. As ganglion cells become necrotic and axons in the RNFL are replaced by a less organized and amorphous tissue composed of glial cells,[1] birefringence changes should be expected to occur. When glaucoma is detected at an early stage, further loss of vision can be prevented by treatment. The visual field test is the current standard method of detecting loss of peripheral vision in glaucoma. However, measurements show that up to 40% of nerves are irreversibly damaged before loss of peripheral vision can be clinically detected.[1]

New instruments have been introduced that determine RNFL thinning. For example, optical coherence tomography (OCT) can produce structural cross sections of the human retina and RNFL.[2] Variations in optical scattering and absorption allow differentiation between the different layers of the retina. A limitation in RNFL thickness determination by OCT is the axial resolution of approximately 10 μm with conventional OCT systems.[3] The difference between high-resolution optical coherence tomography (HR-OCT) and conventional OCT is that HR-OCT uses a light source with a particularly large optical bandwidth, allowing for RNFL thickness measurements with an accuracy of up to 3 μm.[4] However, current ultrabroadband sources are expensive and complex, and because the signal-to-noise ratio of an OCT system is inversely proportional to the detection bandwidth and thus to the source bandwidth, a reduction in acquisition speed is necessary, making HR-OCT less appealing for routine examination.

In scanning laser polarimetry (SLP), the retina in and around the optic nerve head (ONH) is probed with polarized light to detect RNFL phase retardation, which is converted to RNFL thickness.[5,6] The RNFL is slightly birefringent because of its ordered structure,[7] but birefringence is absent in layers that are located below the RNFL, including the ganglion cell layer. Birefringent elements in the eye, such as the cornea and the RNFL, change the polarization state of the incident light. The polarization state of light that is reflected from all retinal structures and that has double passed the RNFL is compared with the input polarization state. Assuming that RNFL birefringence is constant as a function of location and is constant between subjects, RNFL thickness can be calculated from the measured change in the polarization state or the phase retardation of the reflected light.

Polarization-sensitive optical coherence tomography (PS-OCT) combines the depth resolution of OCT with the polarization sensitivity of SLP to image the depth-resolved optical birefringence of biological tissue.[8–13] We hypothesize that glaucomatous loss of nerve fiber tissue may be preceded by a change in birefringence, since it is suspected that disintegration of the nerve fiber mesh leads to a change of RNFL birefringence. Such a change in birefringence compared with normal levels could be an early sign of glaucomatous atrophy of the RNFL. Experiments—for instance, a longitudinal study with PS-OCT on patients at high-risk for development of glaucoma—will either confirm or reject this hypothesis. In addition, PS-OCT may enhance specificity in determining RNFL thickness in structural OCT images by using changes in tissue birefringence to determine the border between the RNFL and ganglion cell layer. Since corneal birefringence changes the incident polar-

From the [1]Harvard Medical School and Wellman Center of Photomedicine, Massachusetts General Hospital, Boston, Massachusetts; and [2]Massachusetts Eye and Ear Infirmary and Harvard Medical School, Boston, Massachusetts.

Supported by National Eye Institute Grant 1R 24 EY 12877, Whitaker Foundation Grant 26083, and a gift from Dr. and Mrs. J. S. Chen to the Optical Diagnostics Program of the Wellman Center of Photomedicine.

Submitted for publication October 21, 2003; revised January 21, March 16, March 26, April 8, and April 12, 2004; accepted April 19, 2004.

Disclosure: **B. Cense**, None; **T.C. Chen**, None; **B.H. Park**, None; **M.C. Pierce**, None; **J.F. de Boer**, (P)

The publication costs of this article were defrayed in part by page charge payment. This article must therefore be marked "*advertisement*" in accordance with 18 U.S.C. §1734 solely to indicate this fact.

Corresponding author: Johannes F. de Boer, Massachusetts General Hospital, Bartlett 726, 50 Blossom Street, Boston, MA 02114; deboer@helix.mgh.harvard.edu.

Investigative Ophthalmology & Visual Science, August 2004, Vol. 45, No. 8

ization state unpredictably,[14] the RNFL surface is used as a reference in the PS-OCT phase retardation calculation. Therefore, our method is insensitive to corneal birefringence.[12,13] In SLP one can compensate for this effect by use of a variable cornea compensator (VCC).[15]

Phase retardation is related to birefringence and RFNL thickness according to the following equation: phase retardation = RNFL birefringence × RNFL thickness. In PS-OCT and SLP the light that scatters back double passes the RNFL before it is detected, which changes the equation to: double-pass phase retardation (DPPR) = RNFL birefringence × 2 × RNFL thickness.

The first in vitro RNFL birefringence measurements were reported by Weinreb et al.[5] With SLP they measured two fixed primate eyes with the anterior segments removed and correlated the measured phase retardation with RNFL thickness histology measurements. They found a typical double-pass phase retardation per unit depth (DPPR/UD) of 0.27 deg/μm. In prior studies, in vivo PS-OCT measurements were performed on the retina of one healthy subject.[12,13] RNFL thickness and depth-resolved birefringence measurements that were obtained in four blocks around the ONH demonstrated that the birefringence or DPPR/UD is not constant, but varies between 0.18 and 0.37 deg/μm (de Boer JF, et al. *IOVS* 2003;44:ARVO E-Abstract 239). Huang et al. (*IOVS* 2003;44:ARVO E-Abstract 235) determined RNFL birefringence using an indirect method combining SLP phase retardation measurements and OCT thickness measurements obtained from healthy volunteers in vivo. Assuming that the measuring beam double passed the RNFL, they found a mean DPPR/UD of 0.37 ± 0.02 deg/μm. In addition, they found that the birefringence varied along a circular path around the ONH, but did not vary as a function of radius or along fiber bundles.

In this study, we obtained detailed RNFL thickness and birefringence measurements in two healthy subjects in vivo. In addition, the accuracy of the system was assessed based on multiple measurements in one of these volunteers. Because the peripapillary RNFL is the most sensitive to changes induced by glaucoma, measurements were obtained in concentric circles around the ONH. This allows determination of the relationship between RNFL thickness and birefringence, and it also gives information on the homogeneity of RNFL birefringence.

Materials and Methods

Experimental Setup

The setup's description (Fig. 1) has been published in detail.[12,13] An axial resolution of 5.9 μm (full width at half maximum [FWHM]) in the retina was obtained with a high-power superluminescent diode (Superlum Diodes, Ltd., Moscow, Russia), assuming an index of refraction of 1.38. The sample arm consisted of a telecentric x– y retina scanner. The incident power on the eye was equal to 495 ± 5 μW, which is well below the ANSI standard limit.[16] A near infrared (NIR)–sensitive charge-coupled device (CCD) camera was connected to the slit lamp setup, equipped with an ophthalmic lens (D60; Volk Optical, Mentor, OH), to visually locate OCT scans in the eye.[13] A fixation spot in the image plane helped volunteers to stabilize their eyes. The reference arm of our system consisted of a rapid-scanning optical-delay line (RSOD).[17] During each circular B-scan of 6 seconds duration, 1536 A-lines over a depth of 1 mm were acquired. Each A-line consisted of 1024 pixels. In real time, both intensity and birefringence B-scans were displayed.[18] The former allowed us to detect the position of the retina in real time. A correction signal was calculated and added to the driving waveform of the RSOD galvanometer, compensating for small shifts of approximately 1 mm due to the volunteer's moving in the direction of depth scanning.

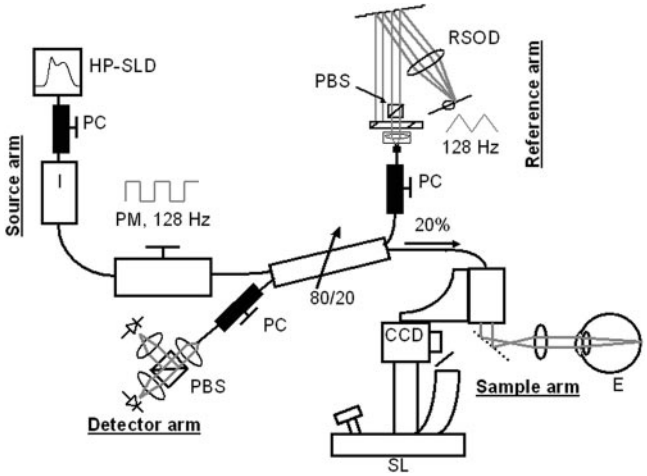

Figure 1. The experimental setup. Light emitted by the super luminescent diode (HP-SLD) was polarized and isolated by means of an isolator (I) and modulated with a polarization modulator (PM) at 128 Hz before it entered a fiber-based 80/20 splitter. The reference arm consisted of an RSOD line. A polarizing beam splitter (PBS) in the RSOD ensured that the reflected power was constant, regardless of the input polarization state. The sample arm contained a slit lamp–based telecentric scanner (SL), which pivoted a beam through the eye's pupil (E) by means of a set of galvanometers and two lenses. In the detector arm, light was split into two orthogonal components by means of a polarizing beam splitter and detected by two silicon detectors. At various locations in the setup, the polarization state could be tuned with polarization controllers (PC).

Volunteer Inclusion and Exclusion Criteria

All experiments were performed under a protocol that adhered to the tenets of the Declaration of Helsinki and was approved by the Institutional Review Boards of both the Massachusetts Eye and Ear Infirmary and Massachusetts General Hospital. For this study, eight volunteers were enrolled. After giving informed consent, subjects underwent a complete ophthalmic examination at the Massachusetts Eye and Ear Infirmary (Boston, MA). This examination included a detailed history, visual acuity testing, intraocular pressure (IOP) measurement, and slit lamp examination. Eyes were dilated with phenylephrine hydrochloride 5.0% and tropicamide 0.8% for a complete retinal examination. Only normal eyes with refractive errors between +5.00 and −5.00 D were included. Subjects were excluded if they had a history of intraocular surgery or laser therapy or had any evidence of retinal disease or glaucoma. Subjects were also excluded if they had occludable angles or any other disease state that would preclude safe pharmacologic pupil dilation. One volunteer was excluded from the study because of evidence of possible early glaucoma. Seven volunteers were accepted and, after pupil dilation, were measured with PS-OCT. After an initial inspection of the data, two data sets with the best signal-to-noise ratio and fewest blinks were selected for detailed data analysis. Data sets were analyzed to determine the accuracy of the system and to map RNFL thickness and birefringence.

Data Analysis

For the RNFL thickness analysis, structural intensity OCT images were corrected for axial motion artifacts, according to a method described by Swanson et al.[19] OCT intensity images were gray-scale encoded on a logarithmic scale, with a white pixel representing low reflectivity and a black pixel indicating high reflectivity. To reduce the influence of speckle noise (grainy noise caused by interference of coherent light), a moving-average filter with a length of ~10 μm was applied in the axial direction. The image of a circular scan was projected as a B-scan and divided into 48 sectors of 32 A-lines, each covering 7.5° of the circular scan starting temporal to the ONH and analyzed with a custom-made program written in commercial software (Visual C++; Microsoft Corp., Redmond, WA).[11,12] In Figure 2, two examples of a combined

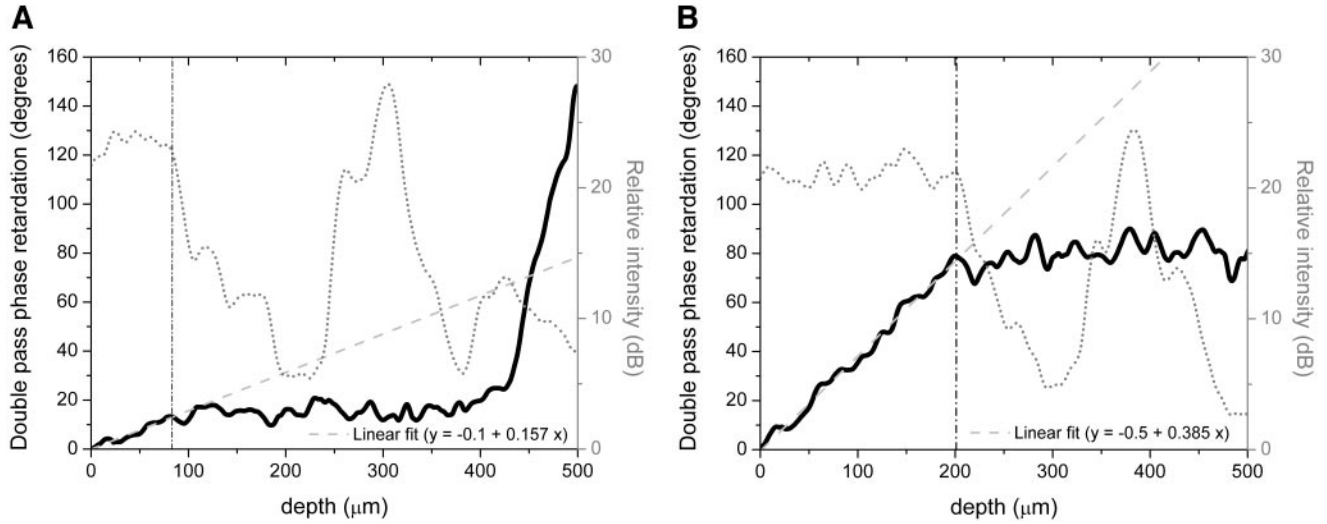

FIGURE 2. Thickness (*dotted line*) and birefringence (*solid line*) plots of an area temporal (**A**) and superior (**B**) to the ONH. DPPR data belonging to the RNFL is fit with a least-squares linear fit. The slope in the equation represents the DPPR/UD or birefringence. The *vertical line* indicates the boundary of the RNFL, as determined from the intensity and DPPR data. In (**A**), the increase in DPPR at a depth beyond 450 μm is caused by either a relatively low signal-to-noise ratio, or by the presence of a highly birefringent material—for instance, collagen in the sclera.

thickness and birefringence measurement are given, one of a sector temporal to the ONH (Fig. 2A), the other of a sector superior to the ONH (Fig. 2B). In these plots, the intensity and double-pass phase retardation averaged over a sector are plotted as a function of depth. A least-squares fit through data points considered to belong to the RNFL is used to calculate the birefringence or DPPR/UD of the RNFL. The RNFL thickness can be determined in two ways. First, a decrease in intensity is a sign of the lesser light-scattering ganglion cell layer and inner plexiform layer deep to the highly light-scattering RNFL tissue. Second, a transition from linearly increasing double-pass phase retardation to a constant level indicates a change from birefringent tissue to tissue without birefringence. The combination of these two methods helps in accurately determining the RNFL boundary. Figure 2 also demonstrates that the RNFL was birefringent, and the retinal layers below the RNFL were not. The birefringence or DPPR/UD is solely determined from the slope of the linear fit through RNFL data points in the double-pass phase retardation plot, which makes this method less dependent on an accurate thickness measurement.[12,13]

The accuracy of the birefringence measurement was evaluated experimentally on a calibrated waveplate and determined to be better than 3%.[13] This number represented the accuracy of the system. In this study, we determined the standard error in the data caused by a combination of speckle noise, biological variation in the sample, and accuracy of the system by repeated measurements on a single eye.

RESULTS

Volunteers

Best corrected visual acuity was 20/20 in both volunteers. Both subjects had intraocular pressure less than 21 mm Hg, a normal-appearing ONH, and normal confrontational visual fields. Volunteer 1 was a 25-year-old white female (left eye) and volunteer 2 was a 39-year-old white male (right eye).

PS-OCT Intensity Images

Figure 3 is a typical example of a structural-intensity OCT image of the retina in the left eye of volunteer 1 obtained with a circular scan with a radius of 2.1 mm around the ONH. The

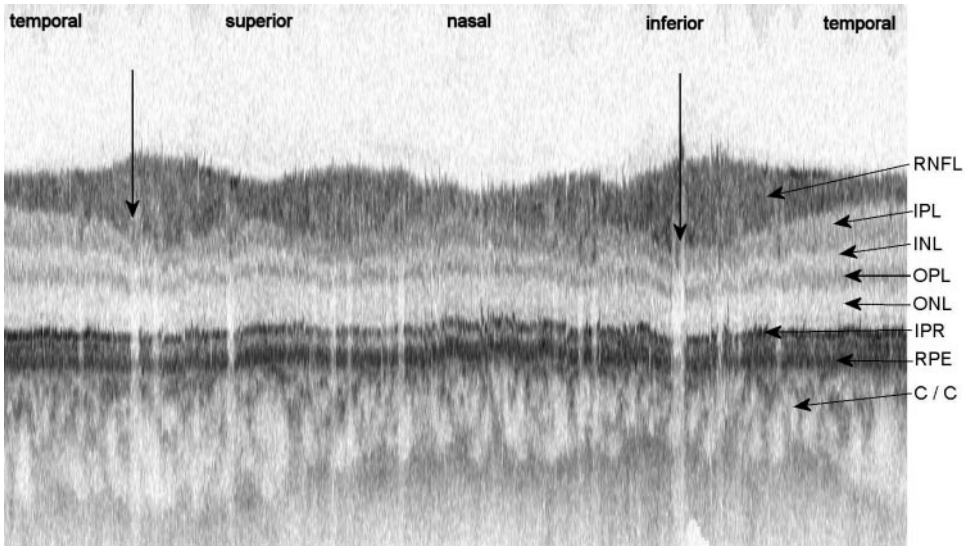

FIGURE 3. A realigned OCT intensity image created with a 2.1-mm radius circular scan around the ONH. The dynamic range of the image is ~36 dB. *Black* pixels represent strong reflections. The image measures 13.3 mm wide and 0.9 mm deep. Visible structures: retinal nerve fiber layer (RNFL); inner plexiform layer (IPL); inner nuclear layer (INL); outer plexiform layer (OPL); outer nuclear layer (ONL); interface between the inner and outer segments of the photoreceptor layer (IPR); retinal pigmented epithelium (RPE); and choriocapillaris and choroid (C/C). *Vertical arrows*: locations of the two largest blood vessels. Other smaller blood vessels appear as *vertical white* areas in the image.

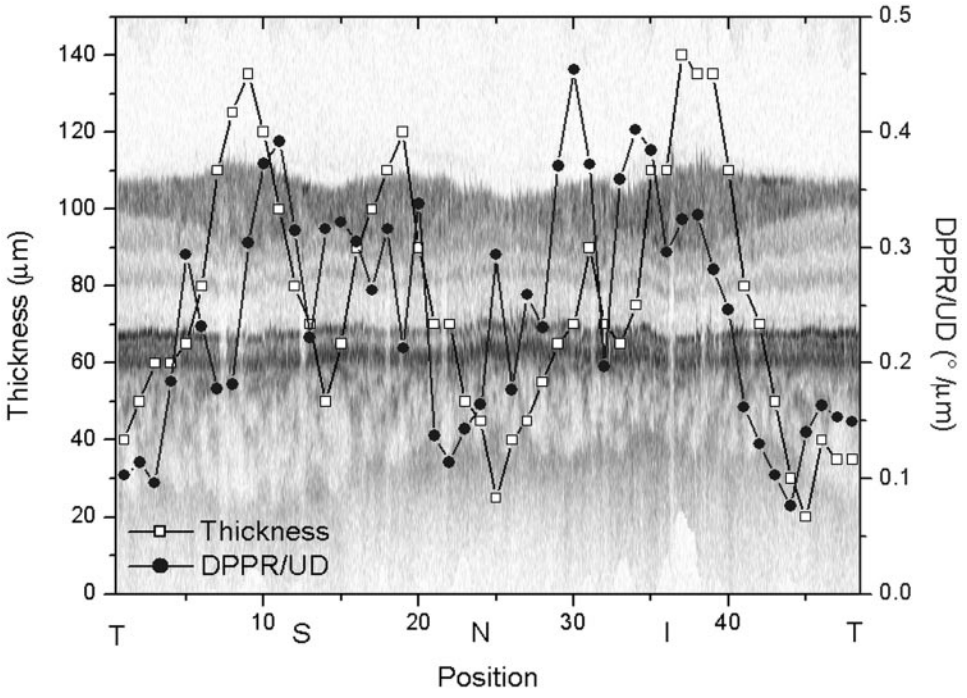

FIGURE 4. A typical example of combined RNFL thickness and birefringence measurements along a circular scan around the ONH. The intensity image is plotted in the background. The RNFL is relatively thicker superiorly (S) and inferiorly (I). A similar development can be seen in the birefringence plot. The birefringence is relatively higher in the thicker areas, whereas it is lower in the thinner temporal (T) and nasal (N) areas.

image measures 13.3 mm wide and 0.9 mm deep and is shown at an expanded aspect ratio in depth for clarity. The dynamic range within the intensity image was approximately 36 dB. For this particular image, speckle noise was removed in each A-line with a moving average filter with a length of ~7 μm in the axial direction. At the left (Fig. 3), the scan starts temporal to the ONH. Structural layers such as the RNFL, the interface between the inner and outer segments of the photoreceptors, and the RPE can be seen.[4]

With our PS-OCT system, thickness *and* birefringence can be measured quantitatively. Figure 4 is a typical example of a combined thickness and birefringence measurement obtained from volunteer 1, with the OCT structural intensity image plotted in the background. RNFL thicknesses and birefringences are displayed as a function of sector of 32 A-lines. The thickness plot indicates that the thickest RNFL was located superiorly and inferiorly. For the birefringence plot, a similar pattern was seen. Birefringence (or DPPR/UD) was relatively high superiorly and inferiorly and lower temporally and nasally.

RNFL Thickness and Birefringence Measurements

Although 12 circular scans were made in each eye, only scans outside the ONH were analyzed. In general, this means that the inner two circular scans that lay inside the ONH were not analyzed.

Thickness. In Figure 5A, RNFL thickness is plotted as a function of sector and scan radius around the ONH of the left

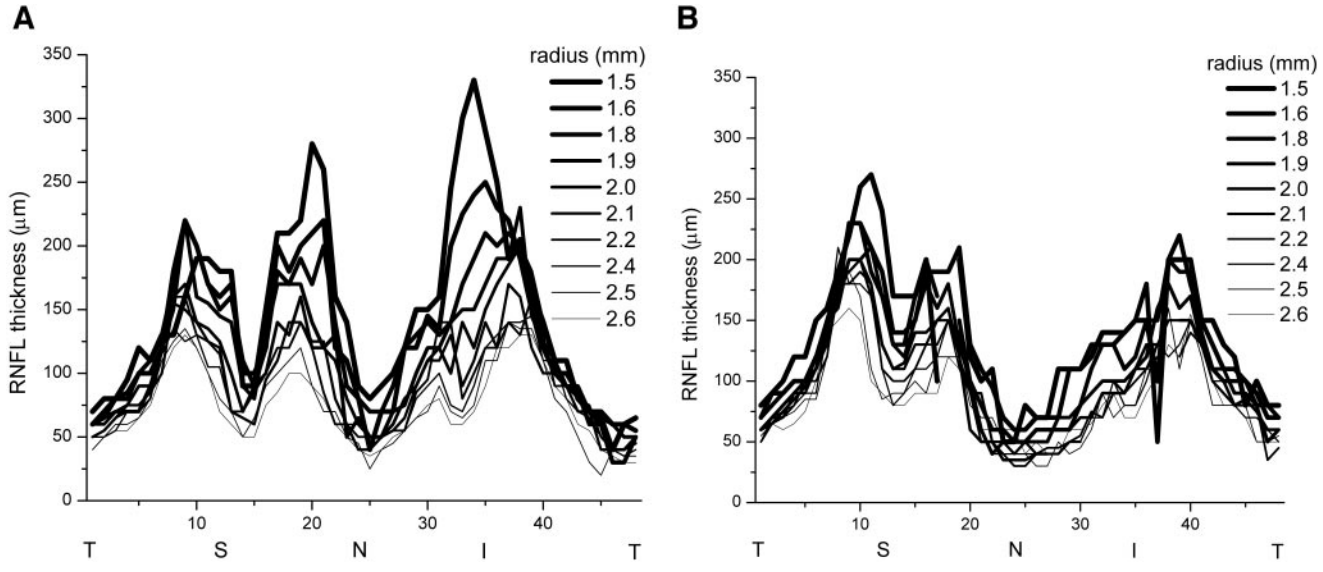

FIGURE 5. RNFL thickness as a function of relative position to and distance from the ONH. (**A**) Left eye of volunteer 1; (**B**) right eye of volunteer 2. RNFL thicknesses are given as a function of position (*x*-axis) and scan radius (*line* style). Positions are relative to the ONH. T, temporal; S, superior; N, nasal; I, inferior.

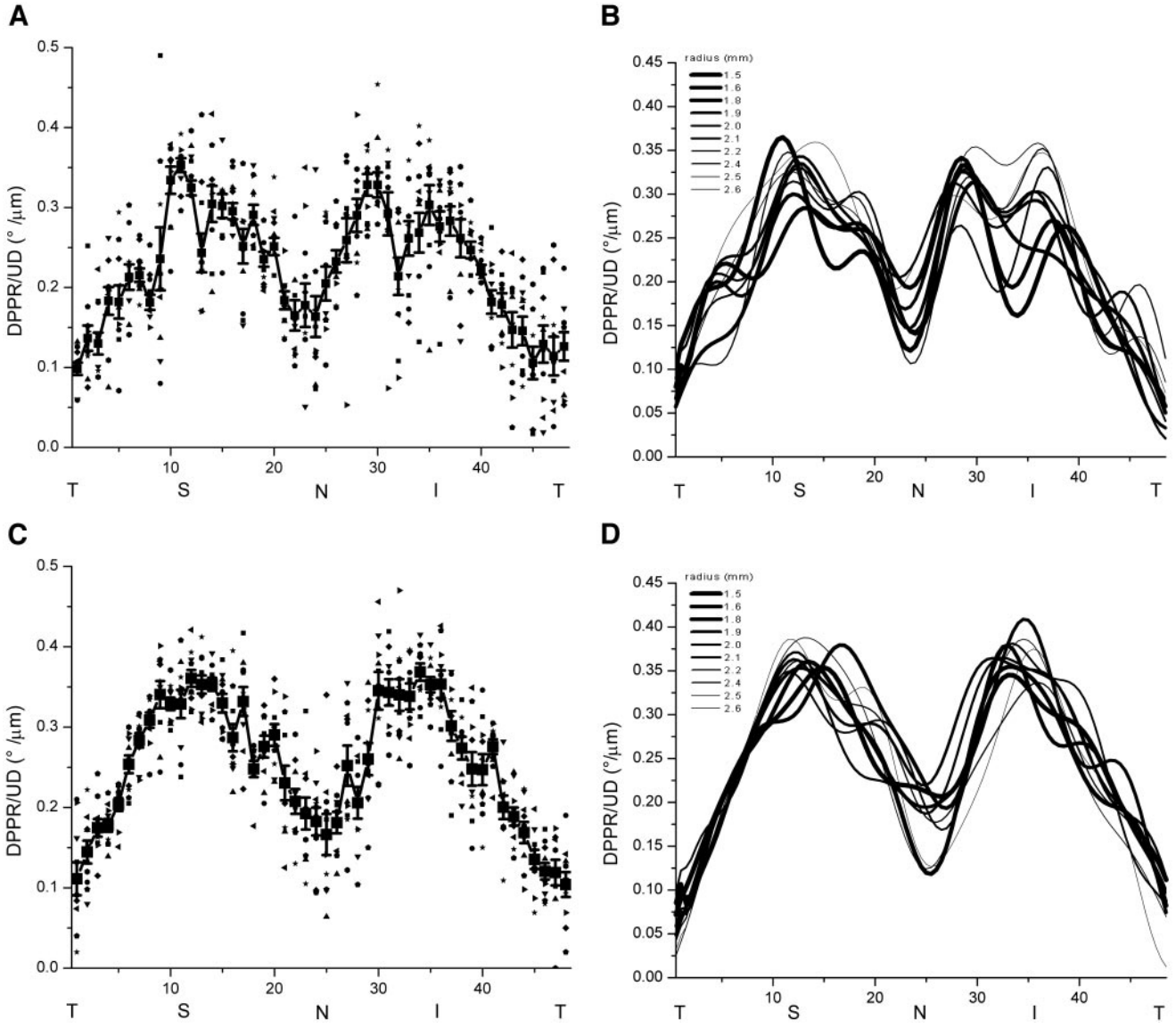

FIGURE 6. (**A**, **C**) the RNFL birefringence is plotted as a function of relative position with respect to the ONH. (**A**, **B**) Left eye of volunteer 1; (**C**, **D**) right eye of volunteer 2. Birefringence was measured in all 48 sectors of 10 scans with radii between 1.5 and 2.6 mm around the ONH. Results from sectors at a certain radius are marked with the same *symbol*. The mean birefringence was marked with a *larger symbol* and connected with a *line*. Error bars, SE. (**B**, **D**) Same data after filtering with a low-pass FFT filter reveals possible trends in DPPR/UD as a function of radius and tells whether averaging is permitted.

eye of volunteer 1. The smallest scan had radius on the retina of 1.5 mm, whereas the largest scan had a radius of 2.6 mm. The different plots demonstrate that an increased distance from the ONH was associated with a thinner RNFL. The thickness variation pattern with higher thicknesses inferior and superior was largely constant as a function of radius. This consistent RNFL thickness pattern can be explained by the fact that most nerves from the retina and fovea enter the ONH inferiorly and superiorly. The data set of volunteer 2 (Fig. 5B) showed characteristics similar to those of the data set of volunteer 1. One major difference is that the RNFL was thickest superior to the ONH of this volunteer.

Using the data sets of volunteer 2, we estimated the thickness measurement error, or standard error, in RNFL thicknesses from three scans with equal radii of 1.8 mm. All three scans were centered similarly on the ONH. Each scan was divided into 48 sectors of equal length. The mean thickness and standard error were calculated for each sector. Involuntary retinal movements created a larger error within sectors in which the thickness varied significantly, compared with sectors with a more uniform thickness. The average standard error of sectors where the RNFL thickness did not change significantly was estimated to be ± 5 μm, but in sectors where the change of thickness was high (e.g., sectors 22 and 32 in Fig. 5A), it was estimated to be ± 10 μm. These errors may vary depending on the amount of eye movement.

Birefringence. The same data sets of volunteers 1 and 2 that were used for the thickness mapping in Figure 5 were analyzed for birefringence information. All measurements per sector of 10 circular scans with increasing radius were plotted as a function of sector. In Figures 6A and 6C (with Fig. 6A containing data of volunteer 1 and volunteer 2 in Fig. 6C) each of 48 measurements at a certain radius is labeled with the same symbol. The mean value per sector and its standard error were plotted and neighboring means were connected with a line. The standard error can be found by dividing the standard deviation by the square root of the number of measurements per sector—in this case, the square root of 10. Averaging over

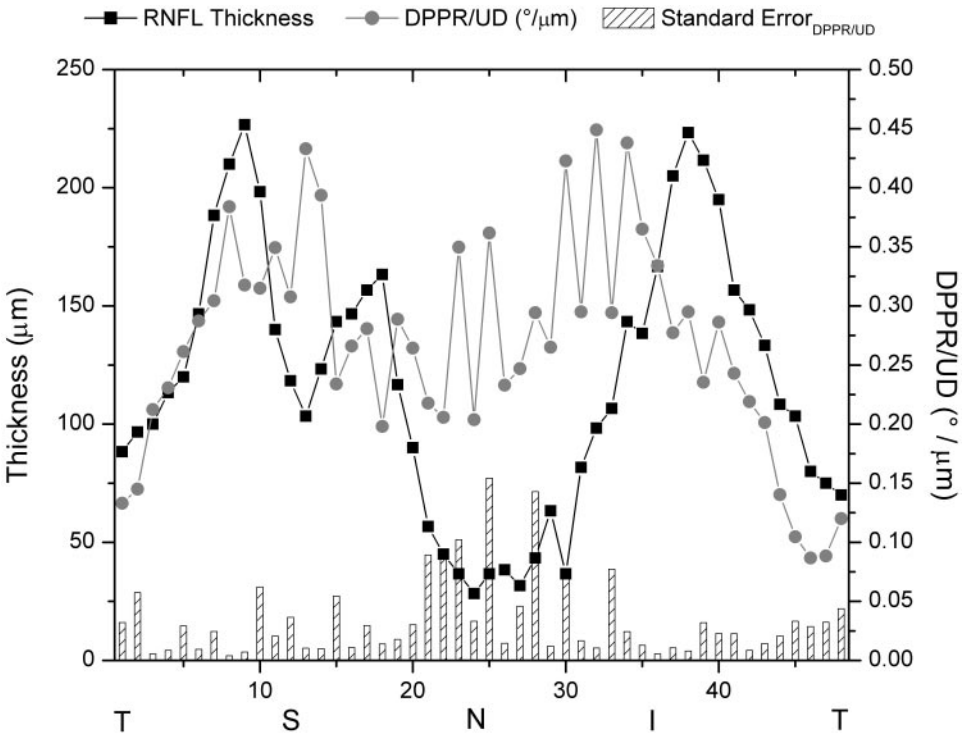

FIGURE 7. The RNFL thickness, average DPPR/UD, and standard error of the DPPR/UD are plotted. In the nasal area, where the thickness was below 75 μm, the DPPR/UD standard error increased, suggesting that birefringence measurements made with the current setup are most reliable in thicker RNFL areas (S and I). Positions are relative to the ONH: T, temporal; S, superior; N, nasal; and I, inferior.

sectors from different radii yields incorrect values when there is a trend as a function of radius. To demonstrate whether averaging is permitted, data sets obtained at different radii were compared with each other. The data in Figure 6 were low-pass filtered with a fast Fourier transform (FFT)–based filter that retained the lowest nine Fourier components. The processed data sets of volunteers 1 and 2 are displayed in Figures 6B and 6D. Thick lines represent filtered data of circular scans closer to the ONH and scans farther away are marked with thinner lines. The processed data set of volunteer 1 indicate an increase of DPPR/UD in the RNFL bundles superiorly and inferiorly around sectors 16 and 36, although a similar trend was not found inferiorly around sector 32. In the data set of volunteer 2, a similar trend was found in the RNFL bundle superiorly. These trends indicate that the means, as displayed in Figures 6A and 6C, do not represent the scans close and far away from the ONH. No trend was observed in the other sectors, which permitted the averaging over sectors.

For both subjects, the birefringence pattern is similar to the thickness pattern. At all scan radii, DPPR/UDs were relatively high in superior and inferior areas. In volunteer 1, the highest DPPR/UD occurred superiorly and was 0.35 $\pm$ 0.03 deg/μm. Volunteer 2's highest DPPR/UD of 0.37 $\pm$ 0.04 deg/μm occurred inferiorly. Both volunteers exhibited low mean measurements in the temporal area: 0.10 $\pm$ 0.03 deg/μm (volunteer 1) and 0.11 $\pm$ 0.05 deg/μm (volunteer 2). For volunteer 1, the difference between the highest and lowest DPPR/UD is equal to 8 SEs, indicating that the observed difference is statistically significant. The same holds for the difference observed in volunteer 2's data, which were more than 5 to 7 SEs apart.

To determine the reliability of the birefringence measurements, three scans repeated with the same radius of 1.8 mm were analyzed. All three scans were obtained in the same eye of volunteer 2 during one measurement session. Figure 7 shows the average RNFL thickness plot combined with a plot of the average DPPR/UD and standard error of the average DPPR/UD to demonstrate the dependence of the DPPR/UD standard error on RNFL thickness. The average standard error in DPPR/UD is approximately $\pm$0.03 deg/μm, except for the thin nasal area, in sectors 20 to 30, where the thickness is below 75 μm. In this area, the average standard error is estimated to be $\pm$0.10 deg/μm. The standard error was found by dividing the SD with the square root of the number of measurements, in this case the square root of 3. The standard errors of Figure 7 (n = 3) and Figure 6 (n = 10) are equivalent.

In areas with blood vessels, birefringence values became less reliable because of attenuation of the signal by the blood. If we had excluded areas encompassing blood vessels, too many sectors would have been excluded. However, blood vessels became smaller and less visible in the intensity images that were taken farther away from the ONH. Some of them sank toward the layer below the RNFL. As a consequence, at a scan radius of 1.8 mm or more, birefringence measurements were less influenced by the presence of blood vessels.

Both volunteer 1 and 2 had lower DPPR/UDs ($\sim$0.10 deg/μm) temporal to the ONH, a value equivalent to a birefringence of 1.2×10^{-4}, measured at a wavelength of 840 nm. Compared with the birefringence of a well-known birefringent material such as collagen, this value is approximately 10 times lower.[20] Superior and inferior higher DPPR/UDs of $\sim$0.35 deg/μm, equivalent to a birefringence of 4.1×10^{-4}, were noted.

DISCUSSION

Our measurements demonstrate that in the healthy retina of two young volunteers, the RNFL birefringence or DPPR/UD varied as a function of sector around the ONH, with the lowest values (0.10 deg/μm) occurring temporally and the highest values ($\sim$0.35 deg/μm) occurring inferiorly and superiorly. In SLP, a constant birefringence or DPPR/UD is used as a conversion factor to convert measured DPPR to RNFL thickness. Because DPPR/UD varies as a function of sector, SLP phase retardation to thickness conversion does not yield accurate RNFL thicknesses in all sectors.

Our DPPR/UD measurement does not rely on an accurate determination of the RNFL thickness. The DPPR/UD is determined from the *slope* of the phase retardation with depth as determined from a PS-OCT depth-resolved phase-retardation measurement.

Weinreb et al.[5] found a correlation between RNFL thickness and phase retardation at different locations in the primate retina, but they did not consider different birefringences as a function of sector, which could explain the considerable variation around the regression line.

Although the RNFL thickness of young healthy subjects may not be measured accurately with SLP, RNFL thinning induced by glaucoma changes the amount of phase retardation, which can be detected with SLP. In addition, phase-retardation changes caused by a change in RNFL birefringence, as we hypothesized earlier, is detected with SLP. With SLP, the combined effect of RNFL thickness and birefringence is measured as a DPPR of the RNFL, which makes it impossible to separate thickness from birefringence. SLP is sensitive to a combination of birefringence change and thickness change. PS-OCT measures RNFL thickness and the depth-resolved birefringence simultaneously. Our data do not invalidate the clinical value of a phase-retardation measurement, such as is obtained with SLP, but affects the conversion of phase-retardation to RNFL thickness.

Conclusions

Birefringence of healthy RNFL is constant as a function of scan radius but varies as a function of position around the ONH, with higher values occurring superior and inferior to the ONH. Measured DPPR/UDs around the ONH in two healthy subjects varied between 0.10 and 0.35 deg/μm. These values are equivalent to birefringences of 1.2×10^{-4} and 4.1×10^{-4}, measured at a wavelength of 840 nm. Consequently, when assuming a spatially constant birefringence around the ONH, the conversion of SLP phase retardation measurements may yield incorrect thicknesses.

References

1. Quigley HA, Addicks EM, Green WR. Optic nerve damage in human glaucoma. III. Quantitative correlation of nerve fiber loss and visual field defect in glaucoma, ischemic neuropathy, papilledema, and toxic neuropathy. *Arch Ophthalmol.* 1982:100:135–146.
2. Huang D, Swanson EA, Lin CP, et al. Optical coherence tomography. *Science*. 1991;254:1178–1181.
3. Schuman JS, Hee MR, Puliafito CA, et al. Quantification of nerve fiber layer thickness in normal and glaucomatous eyes using optical coherence tomography. *Arch Ophthalmol.* 1995;113:586–596.
4. Drexler W, Sattmann H, Hermann B, et al. Enhanced visualization of macular pathology with the use of ultrahigh-resolution optical coherence tomography. *Arch Ophthalmol.* 2003;121:695–706.
5. Weinreb RN, Dreher AW, Coleman A, et al. Histopathologic validation of Fourier-ellipsometry measurements of retinal nerve fiber layer thickness. *Arch Ophthalmol.* 1990;108:557–560.
6. Weinreb RN, Bowd C, Zangwill LM. Glaucoma detection using scanning laser polarimetry with variable corneal polarization compensation. *Arch Ophthalmol.* 2003;121:218–224.
7. Zhou Q, Knighton RW. Light scattering and form birefringence of parallel cylindrical arrays that represent cellular organelles of the retinal nerve fiber layer. *Appl Opt.* 1997;36:2273–2285.
8. de Boer JF, Milner TE, van Gemert MJC, Nelson JS. Two-dimensional birefringence imaging in biological tissue by polarization-sensitive optical coherence tomography. *Opt Lett.* 1997;22:934–936.
9. de Boer JF, Milner TE, Nelson JS. Determination of the depth-resolved Stokes parameters of light backscattered from turbid media by use of polarization-sensitive optical coherence tomography. *Opt Lett*. 1999;24:300–302.
10. Saxer CE, de Boer JF, Park BH, et al. High-speed fiber-based polarization-sensitive optical coherence tomography of in vivo human skin. *Opt Lett.* 2000;25:1355–1357.
11. Park BH, Saxer C, Srinivas SM, Nelson JS, de Boer JF. In vivo burn depth determination by high-speed fiber-based polarization sensitive optical coherence tomography. *J Biomed Opt.* 2001;6:474–479.
12. Cense B, Chen TC, Park BH, Pierce MC, de Boer JF. In vivo depth-resolved birefringence measurements of the human retinal nerve fiber layer by polarization-sensitive optical coherence tomography. *Opt Lett.* 2002;27:1610–1612.
13. Cense B, Chen TC, Park BH, Pierce MC, de Boer JF . In vivo birefringence and thickness measurements of the human retinal nerve fiber layer using polarization-sensitive optical coherence tomography. *J Biomed Opt.* 2004;9:121–125.
14. Greenfield DS, Knighton RW, Huang X. Effect of corneal polarization on scanning laser polarimetry measurements. *Am J Ophthalmol.* 2000;129:715–722.
15. Zhou QY, Weinreb RN. Individualized compensation of anterior segment birefringence during scanning laser polarimetry. *Invest Ophthalmol Vis Sci.* 2002;43:2221–2228.
16. American National Standards Institute. *American National Standard for Safe Use of Lasers Z136.1.* Orlando, FL: American National Standards Institute; 2000:35–38.
17. Tearney GJ, Bouma BE, Fujimoto JG. High-speed phase- and group-delay scanning with a grating-based phase control delay line. *Opt Lett.* 1997;22:1811–1813.
18. Park BH, Pierce MC, Cense B, de Boer JF. Real-time multi-functional optical coherence tomography. *Opt Express.* 2003;11:782–793.
19. Swanson EA, Izatt JA, Hee MR, et al. In-vivo retinal imaging by optical coherence tomography. *Opt Lett.* 1993;18:1864–1866.
20. Maitland DJ, Walsh JT. Quantitative measurements of linear birefringence during heating of native collagen. *Lasers Surg Med.* 1997;20:310–318.